Chapter 2

Simulation and fabrication of metal nanostructures to study coupled LSPR field magnitude for SERS based sensing investigation

---

In this chapter, simulation study of metal nanostructures that supports strong LSPR field has been discussed. Fabrication of the optimized structure using EBL technique and its subsequent use as SERS substrate for detection of an analyte sample has been discussed.

2.1 Introduction

The key to the enhancement of Raman signal is the LSPR, which is a phenomenon that occurs due to strong EM field coupling with metal nanostructures upon interaction of the incident laser light on it. The spatially confined EM field scatters strong Raman signal when a Raman active sample is brought to the vicinity of the metal nanostructures. The LSPR field condition is greatly affected by size, shape and spacing of metal nanostructure which eventually influences on average enhancement of Raman signals scatter from the sample. To generate strong LSPR field, metal nanostructures of different size, shape have been obtained by wet chemical and/or lithographic techniques. Generation of different nanostructures of different sizes for optimum LSPR field condition is expensive, time consuming and complex. Therefore, it is not always possible to ob-

tain a nanostructure experimentally and looking for optimum LSPR condition. Under this circumstance simulating different structures using commercially available simulation tools, and optimizing the structure that supports maximum LSPR field coupling condition could minimize time and cost to the lowest possible. In recent years LSPR field condition study in metal nanostructure has become an important area for different fields of applications which include chemical and biosensing investigations. Due to its ability to generate highly enhanced LSPR field condition in the vicinity of the patterned nanostructures, last two decades have witnessed the extensive study of patterned metal nanostructures. Such enhancements are results from the confinement in electromagnetic field at very close proximity of the metallic nanostructure. In the recent past extensive research works on LSPR based sensing investigations which have covered a wide field of applications spanning from biomolecular sensing [1-6] to different chemicals and gas sensing [4, 7, 8] have been carried out. The carefully engineered metal nanostructure in which EM field strongly couples with the nanostructure by enhancing the LSPR field condition is the key to the popularity of LSPR based sensing investigation, in particular, to SERS based sensing study. Different shapes and patterns such as nanodomes, nanorods, bow-tie etc. shaped nanostructures [9-18] have been studied to generate enhanced LSPR field coupling conditions. In this chapter simulation study of two new nanostructures have been discussed thoroughly. One of these structure has been fabricated using EBL technique and subsequently demonstrated for SERS based sensing studies.

2.2 Design of metal nanostructure for maximum LSPR field condition

Brief overview of simulation tool

Throughout the thesis work, all the simulation studies have been carried out using COMSOL multiphysics software (wave optic module). This specific simulation tool is based on finite element method, i.e. it solves the problem using partial differential equations. This method considers the piecewise continuous function for the solution and obtains the parameters of the function in a manner that reduces the error in the solution. It has some built-in physics mode, so it is possible to build a model just by defining its physical quantities such as material properties, loads, constraints, sources and fluxes rather than by defining the underlying equations [19]. The wave optic module is used to compute electric and magnetic field for systems where the wavelength is comparable to or much smaller than the studied system.

2.2.1 Periodically varying height Au nanopillar

Owing to its high aspect ratio, pillar-like nanostructure are useful for different SERS based sensing investigations. Furthermore, metal nanopillar structures generate LSPR in the near-infrared (NIR) region [20-22]. In this wavelength region the affect of fluorescence emissions on the Raman signals of many important chemicals can be avoided. Magnitude of the generated LSPR field condition in the structure depends on many factors such as pillar diameter, gap between the pillars and refractive index of surrounding medium. The roughness of the structure also influences the LSPR field coupling condition and so in SERS signal intensities. Due to the fact that the structural roughness in the nanopatterns could modify the coupling cross section, a periodically varying height Au nanopillars structure has been considered for this study. The obtained results are compared to that of uniform pillar height Au nanopillars. Figure 2.1 shows the schematic representation of a periodically varying height gold nanopillar structure patterned on silica (SiO_2) substrate.

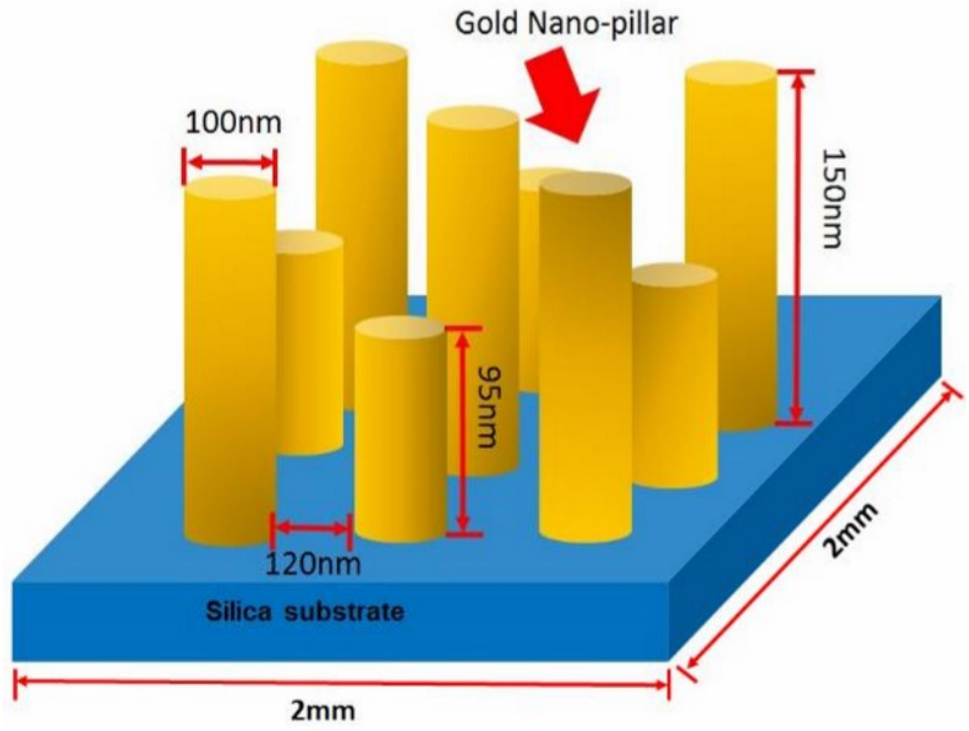

Figure 2.1: Schematic of a periodically varying height gold nanopillar structure patterned on silica (SiO_2) substrate

LSPR field profile for uniform and periodically varying height Au nanopillar

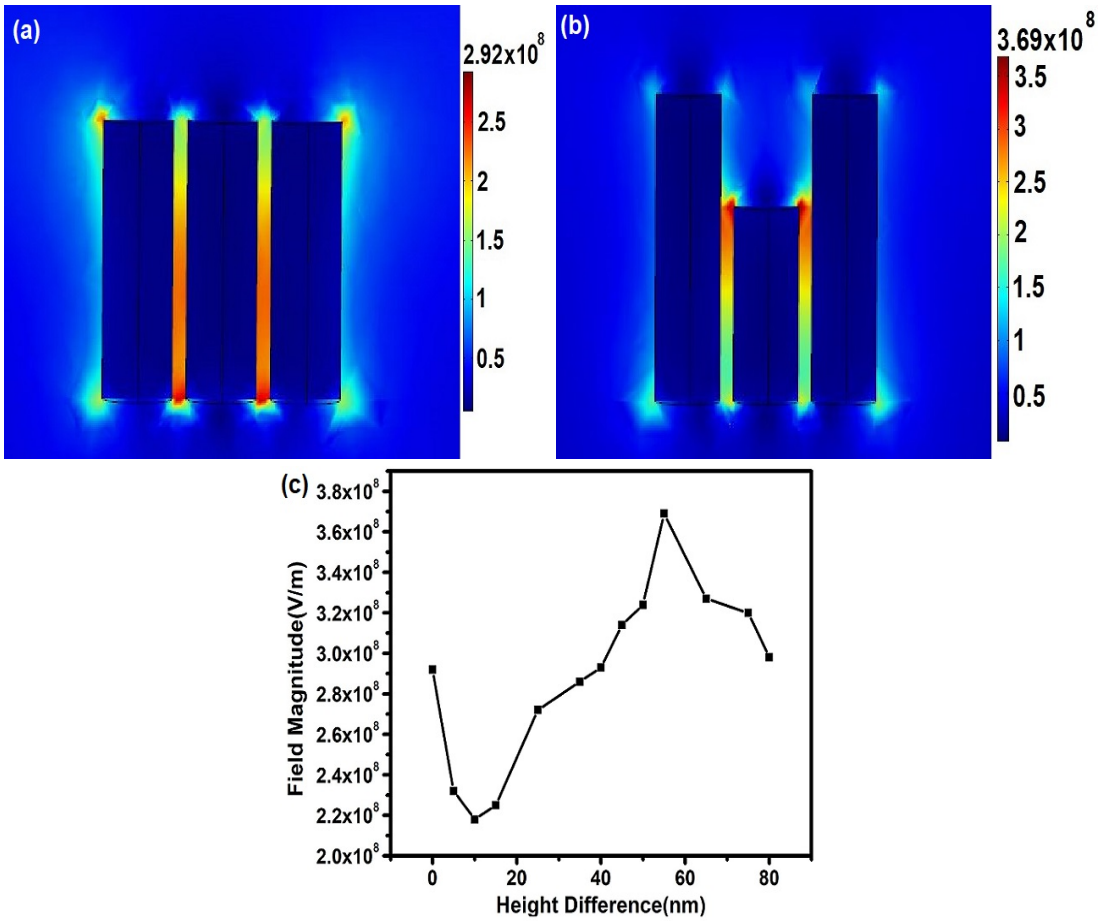

Figure 2.2: Simulation result of Au nanopillar for (a) pillars with no height difference and (b) pillars with height difference of 55nm. We maintain fixed pillar diameter of 50 nm and separation of 10 nm for both the situations. (c) Characteristic curve that represents generated LSPR field conditions for Au nanopillar structures at different pillar height differences.

To study the LSPR field condition in the proposed structure, Au nanopillars are considered on silica substrate. Frequency-dependent complex dielectric function for Au has been considered in the present study [23]. At first, uniformly structured Au nanopillars with pillar height of 150 nm, diameter of 50 nm, and interpillar separation of 10 nm have been considered. Study of LSPR field condition for this structure has been performed for normally incident plane polarized laser source of wavelength 785 nm. Maximum LSPR field condition for this structure is observed to be 2.92×10^8 V/m for the incident electric field of 4.42×10^7 V/m. For the same structural parameters, the height of the pillars has been varied periodically and the LSPR field coupling conditions are studied. Figure 2.2 (a) and (b) shows the simulation results for uniformly patterned Au nanopillars structure and periodically varying height Au nanopillars structures with

pillar height difference of 55 nm. Figure 2.2 (c) shows the characteristic curve showing the variation of LSPR field condition with change in height difference for all the considered patterned structures in the present simulation study. For all the structures same spacing of 10 nm and pillar diameter of 50 nm have been maintained. It has been observed that among the considered patterns, Au nanopillars with pillar height difference of 55 nm yields the maximum LSPR field condition with the value of 3.69×10^8 V/m and compared to uniform pillar height structure, the LSPR field magnitude is enhanced by factor of 1.26 for the periodically varying height metal nanopillar. This enhancement of LSPR field condition is attributed to the increase in effective cross section of the coupling EM field of the incident electromagnetic wave with the patterned structure.

LSPR field for different diameter nanopillar

Upon optimizing the pillar height difference, for which the proposed Au nanopillar structure generates a maximum LSPR field coupling condition, further study has been carried out for different pillar diameters. Maintaining fixed pillar height difference of 55 nm and spacing of 10 nm, the LSPR field condition has been studied for pillar diameters ranging from 50 to 160 nm with a step increment of 10 nm. Figure 2.3 (a)-(c) shows three of the simulation results for pillar diameters of 50, 100 and 120 nm respectively. Figure 2.3 (d) illustrates the characteristic curve of LSPR field condition for different pillar diameter variations while maintaining a fixed pillar height difference and spacing. Among the considered patterns, the maximum LSPR field magnitude of 1.34×10^9 V/m has been observed corresponding to pillar diameter of 100 nm. The coupled field magnitude is found to be enhanced by a factor of 1.19 compared to its uniformly patterned counterpart. This optimum LSPR field condition for 100 nm pillar diameter is again attributed to optimum coupling condition of the incident field for this structure. Beyond 100 nm pillar diameter, the LSPR field condition is observed to be decreasing gradually with the diameter of metal nanopillar.

LSPR field for interpillar spacing

To study the effect of pillar spacing on the coupled LSPR field condition, seven sets of periodic structures have been considered at different interpillar spacing ranging from 10 to 50 nm and maintaining a same pillar height difference i.e. 55 nm. The characteristic LSPR field condition for the considered sets of different pillar diameters is shown in figure 2.4. Clearly, from this characteristic curve it is observed that with the increase of

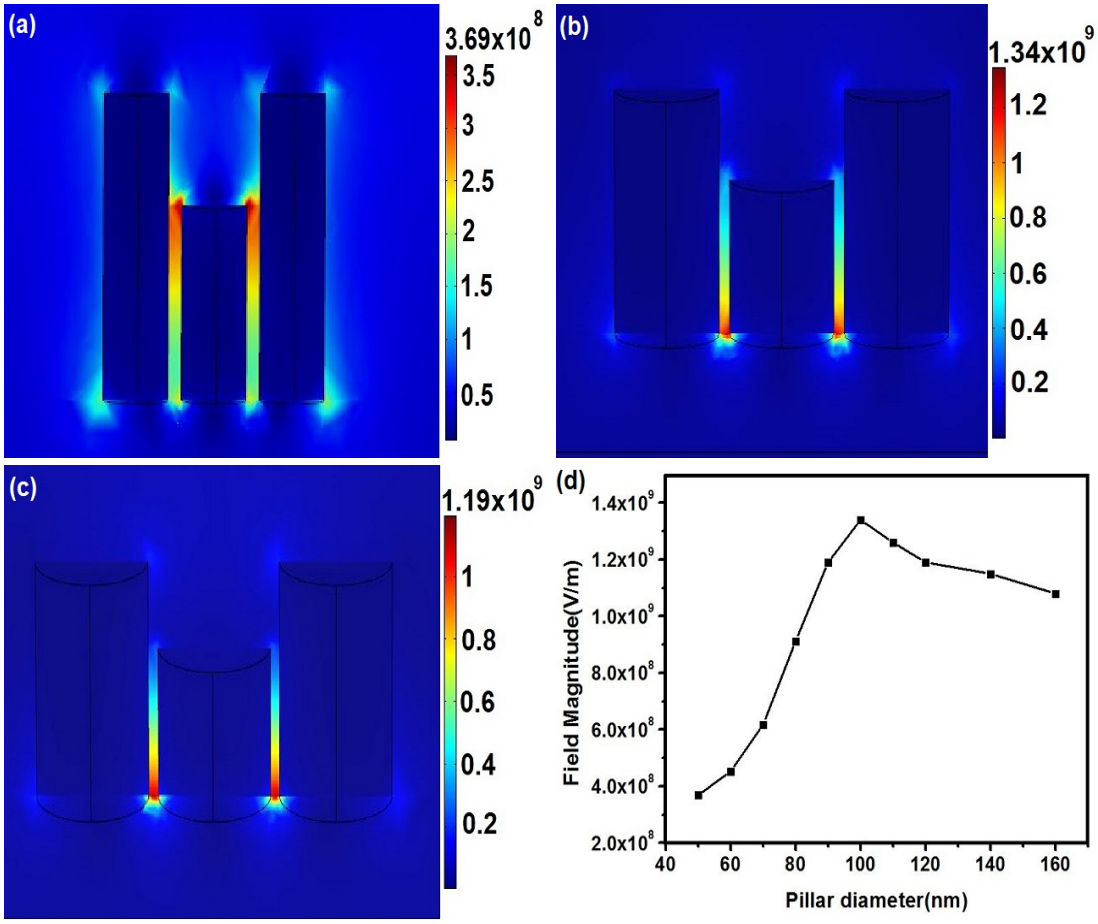

Figure 2.3: Simulation results of the generated LSPR field conditions for different pillar diameters of the proposed periodic Au nanopillar structures. (a) 50 nm, (b) 100 nmand (c) 120 nmpillar diameter. In all the considered cases, we maintain a constant pillar height difference of 55 nm and spacing of 10 nm (d) representing the characteristic curve of LSPR field conditions for different pillar diameter periodically varying height Au nanopillar structures.

interpillar spacing, the magnitude of LSPR field falls off rapidly. The optimum LSPR field condition is observed for AuNP with diameter 100 nm at pillar spacing of 10 nm. The optimum field coupling condition for this structure is again attributed to the optimum cross section of the incident electromagnetic wave with the designed structure which generates the highest LSPR field magnitude among all the structure.

Generated LSPR field dependence on incident wavelength

For effective generation of LSPR condition, the excitation frequency of the incident EM wave should match the resonance oscillation frequency of the nanostructure. SERS based investigations are usually studied for excitation laser source of wavelength 532 nm, 614

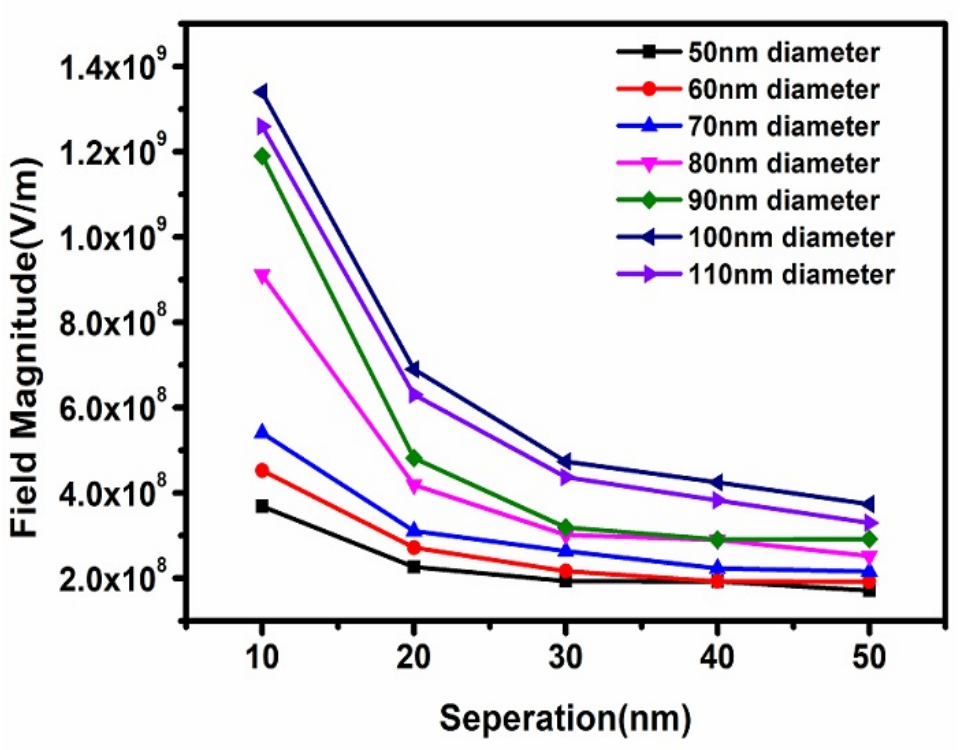

Figure 2.4: Characteristic curve of separation vs maximum field intensity for pillar diameter periodically varying height Au nanopillar structures ranging from 50 to 110 nm at a height difference of 55 nm.

nm, 633 nm and 785 nm. In the present study, the dependence of field coupling condition of the excitation source with the metal nanostructure has been evaluated for different incident wavelength source. Here, metal nanopillar of diameter 100 nm with height difference of 55 nm having interpillar separation of 10 nm has been maintained. Figure 2.5 shows the characteristic LSPR field magnitude for different incident laser source. The maximum field coupling condition is observed at 614 nm which is again attributed to the optimum conditions for resonance coupling of the EM field with the considered pattern in the present study.

Comparison of LSPR field between periodically varying height and uniform height Au nanopillar structures

When the height of the nanopillar varies in the structure, the roughness in the structure would increase which eventually increase the effective coupling cross section of EM radiation with the structure. This would lead to enhancement of LSPR field magnitude. A series of simulation studies have been carried out to compare the generated LSPR field magnitude between periodically varying height and uniform height Au nanopillar

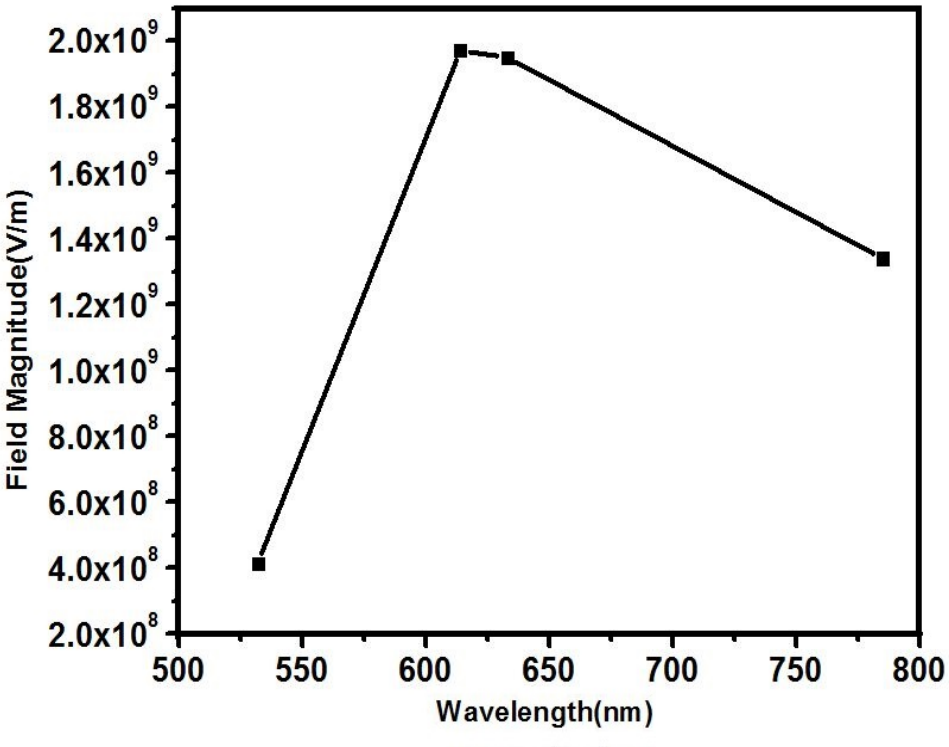

Figure 2.5: Characteristic curve representing the LSPR field magnitudes for different incident laser source wavelength for a same periodically varying height Au nanopillar structure.

structure at different pillar diameter and interpillar spacing. Table 2.1 summarizes the corresponding results of this study. For all considered situations, an enhancement in the LSPR field magnitude has been observed for the proposed structure as compared to uniformly patterned Au nanopillar structure.

Table 2.1: Maximum LSPR field magnitude for uniform height and periodically varying height Au nanopillar structures

Diameter (nm)	**Uniform Au nanopillar structure ($\times 10^8$ V/m)**			**Periodic Au nanopillar structure ($\times 10^8$ V/m)**		
	10 nm separation	**20 nm separation**	**30 nm separation**	**10 nm separation**	**20 nm separatio**	**30 nm separation**
50	2.92	1.89	1.59	3.69	2.27	1.94
60	3.69	2.69	2.1	4.53	2.72	2.17
70	5.13	2.68	2.5	6.18	3.4	2.69
80	6.89	3.76	3.17	9.12	4.19	3.02
90	9.87	4.44	3.23	11.9	4.82	3.19
100	11.2	2.29	3.56	13.4	6.9	4.74
110	12.4	5.81	4.02	12.6	6.31	4.37

2.2.2 Design of diagonally aligned squared Au nanostructure and simulation study

The intensity of coupled electric field at the sharp edges of metal nanostructure is found to be enhanced compared to the flat edges, which is termed as lightning rod effect [24]. Taking the advantage of this effect, another nanostructure of squared Au nanopillar has been considered in the present study, where the squared metal nanostructures are aligned diagonally. In this structure, coupled electromagnetic field would be localized strongly at the gap of the sharp edge between two nearby metal pillars. The strongly localized field would scatter intense Raman signal when a Raman active substance is brought to the vicinity of the sharp edges. The schematic of the proposed metal nanostructure is shown in figure 2.6 (a).

Simulation

The LSPR field coupling condition for the proposed diagonally aligned squared Au nanopillar (DASAuNP) structure has been studied using the simulation tool. Here, the DASAuNPs are designed on SiO_2 base with pillar side length varying between 180 nm to 250 nm in step incremental value of 10 nm and the interpillar spacing is varying between 60 nm to 130 nm with 10 nm step increment. A plane polarized light of wavelength 785 nm is defined as an excitation source and is allowed to incident normally on the structure. Figure 2.6 (b) shows the characteristic curves of the coupled LSPR field magnitudes for different side length and interpillar spacing of the DASAuNP structure. The side and top view of LSPR field distribution around the nanopillar as obtained from the simulation study of the patterned structure is shown in figure 2.6 (c) and (d) respectively. As evident from figure 2.6 (b), the generated LSPR field magnitude is observed to be random with respect to the spacing and side length of the structure. This is attributed to the optimum field coupling condition for different DASAuNP structures is different for the same incident EM wave. The coupled LSPR field magnitude is different at different positions of the structure.

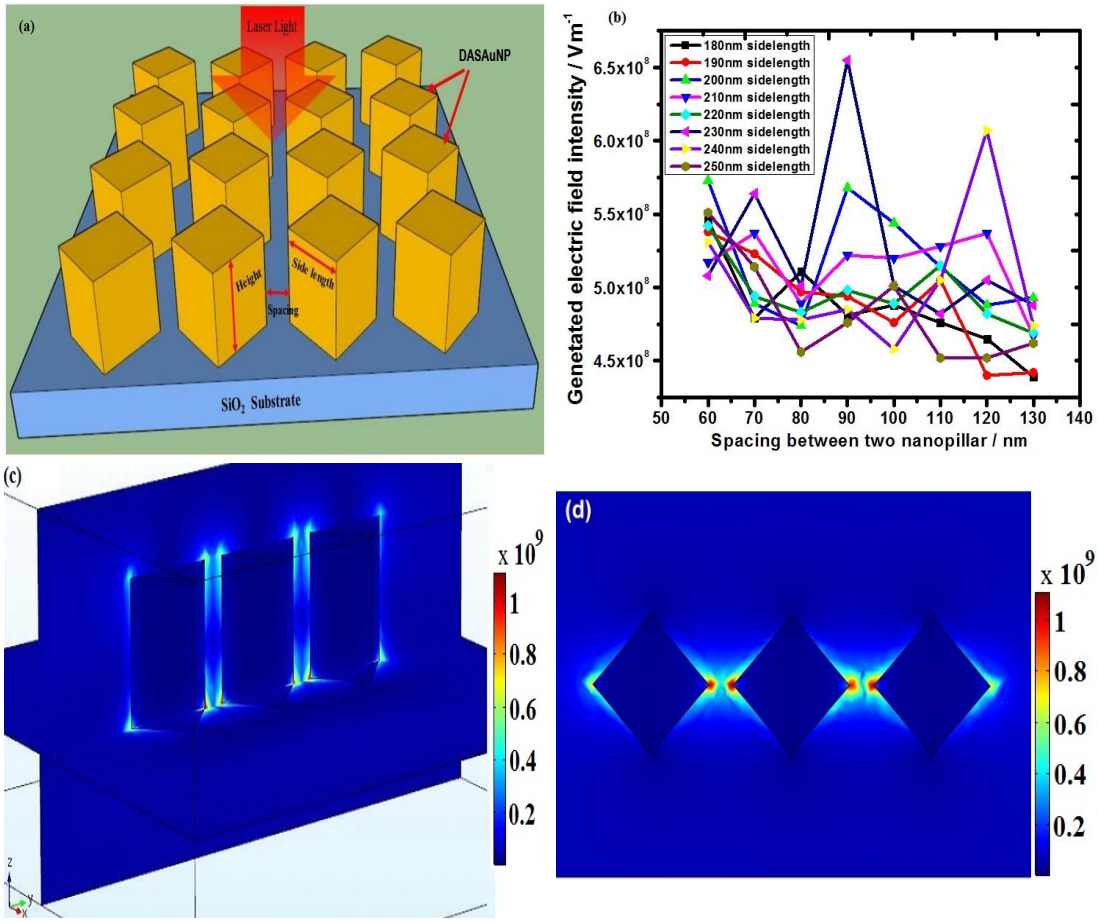

Figure 2.6: (a) Schematic diagram of DASAuNP arrangement, (b) characteristic curve of generated LSPR field magnitude vs internanoparticle spacing for different nanoparticle side length, (c) and (d) Side and top view of FEM simulation result of LSPR field distribution obtained by considering dimensions taken from SEM images.

2.3 Fabrication of nanostructure

Out of the two considered nanostructures namely periodically varying height Au nanopillar and DASAuNP, the DASAuNP structure has been fabricated on SiO_2 grown Si substrate using EBL technique. SERS based sensing investigation of the fabricated SERS substrate has been performed. In the following subsections, details of the fabrication of the proposed substrate and its application for Raman sensing studies are discussed. Important sensorstic parameters have also been evaluated for the fabricated substrate.

2.3.1 Experimental

Fabrication of SERS substrate

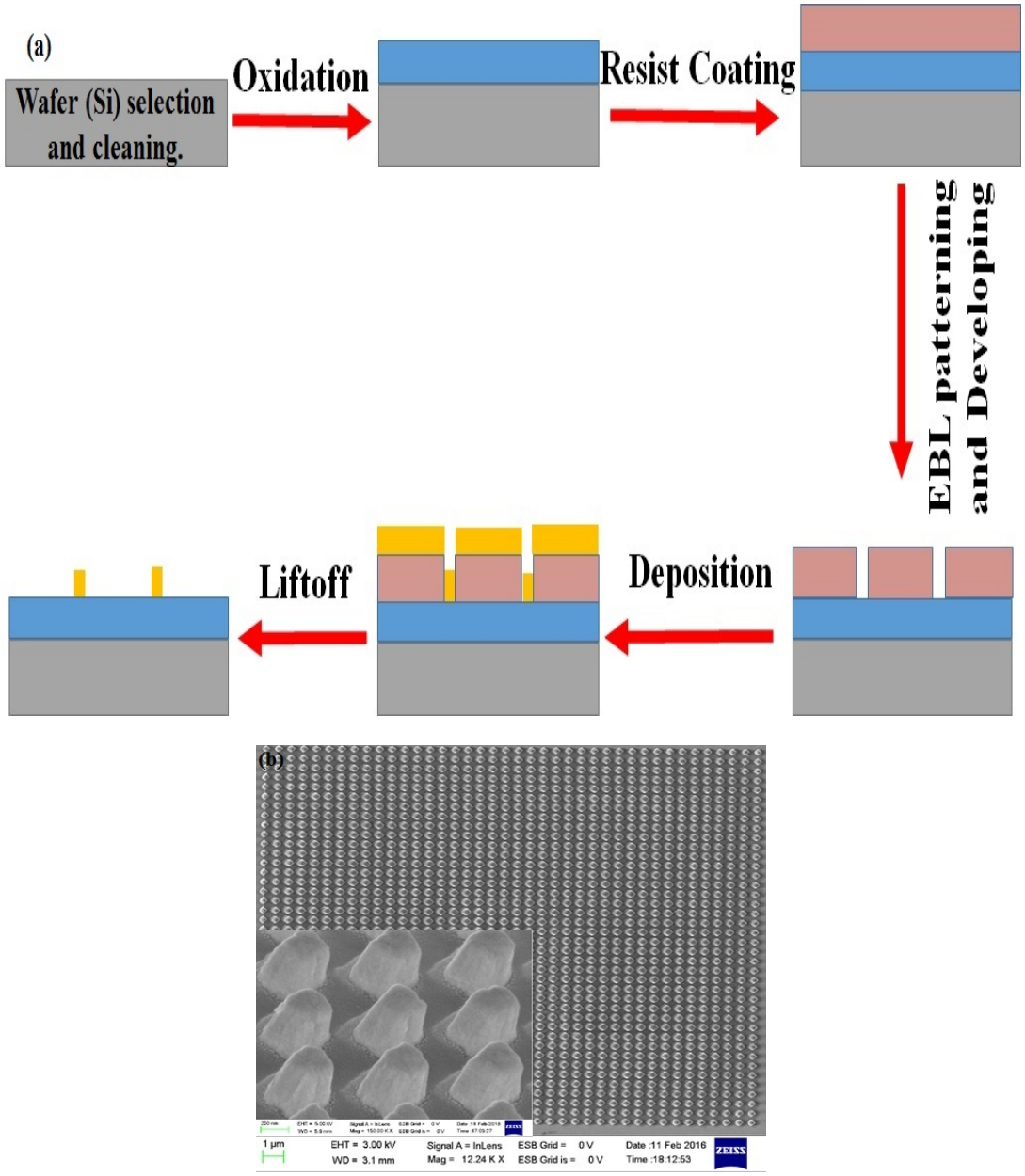

Figure 2.7: (a) Steps involved in fabrication of DASAuNP. (b) Top view of fabricated diagonally aligned squared gold nanopillar, and the inset image shows the enlarge and tilted view of the nanopillars.

To fabricate the DASAuNP substrate, initially the silicon wafer is RCA cleaned and then put into a wet oxidation furnace for oxidation. The oxidized wafer is then cut into small pieces followed by acetone and isopropyl alcohol (IPA) bath. A bilayer of

Polymethyl methacrylate (PMMA) (PMMA 495 A4 at 3000 rpm and PMMA 950 A4 at 3000 rpm) is coated on the substrate. The PMMA layer acts as a resist in the present case. Using electron beam lithographic tool (Raith 150 two) the desired pattern has been written on the PMMA coated substrate. Upon completion of writing, the substrate is developed in 1:3 MIBK/IPA for 60 seconds, followed by IPA treatment for 20 seconds. For better adhesion of Au on the substrate, 10 nm chromium (Cr) has been deposited on the substrate followed by deposition of 190 nm Au. Both Cr and Au have been deposited using thermal evaporator (Hind HiVac 12A40) at a rate of 0.3 and 0.8 $\mathring{A}$/s, respectively. The Au deposited sample is then liftoff, and the pattern has been observed under scanning electron microscope (Zeiss Ultra 55 FESEM). The process flow of the fabrication steps to obtain the patterned DASAuNP structure is shown in figure 2.7 (a). Figure 2.7 (b) shows the FESEM image of one such fabricated pattern obtained from above steps. The inset image shows the zoom-in and tilted view of the patterned structure.

Raman measurement

Throughout the thesis work, for detection and analysis of the Raman signals, Raman spectrometer from Enwave optronics, USA (EZRaman-N) has been used. This spectrometer is equipped with a diode laser with excitation wavelength of 785 nm. The spectrometer houses a thermoelectric temperature controlled CCD detector having pixel resolution of 0.1 cm^{-1} per pixel. Light signal from the laser source is guided by an optical fiber and an objective lens (numerical aperture 0.22) to the sample and back-scattered Raman signal from the sample is collected by the same fiber and guided to the detection unit of the spectrometer by the guiding optics.

Analyte sample preparation

RhodamineB (RhB) stock solution of concentration 10 mM has been prepared in distilled water (DI) by adding proportional amount of RhB into it. Different concentrations of RhB samples can be obtained by diluting the stock solution with DI water. To study the Raman signal intensity for this Raman active sample, 10 μL of the sample is pipetted on the SERS substrate and the back scattered signal is recorded by a Raman spectrometer.

2.4 Results and discussion

2.4.1 Characterization of the substrate

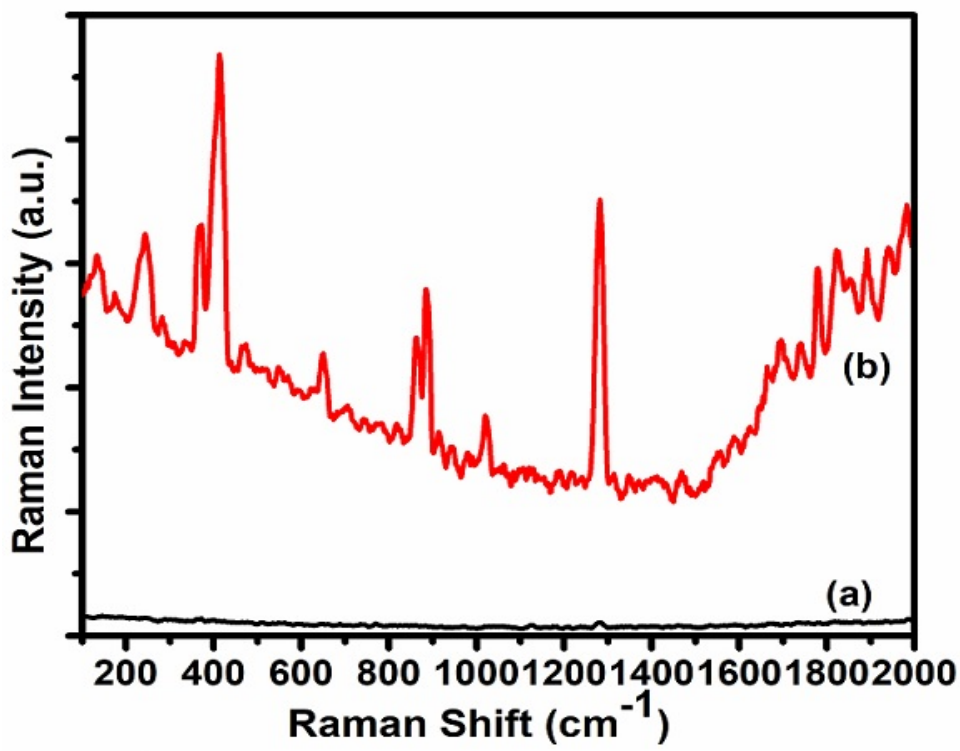

Figure 2.8: Comparison of Raman spectra of RhB between plane silica substrate and DASAuNP substrate. (a) For 1 mM RhB solution on plane silica substrate, the signal was magnified by 20 times (b) For 1 μM RhB solution on DASAuNP substrate.

To evaluate the field enhancement of the SERS substrate, 1 μM and 1 mM of RhB samples have been treated separately on the designed SERS substrate and plan silicon substrate respectively and allowed to dry at room temperature. Upon drying of the sample, the back scattered Raman signal of RhB scattered from the substrates are recorded. Figure 2.8 illustrates the characteristic Raman signals recorded by spectrometer for these two different situations. Clearly, as compared to a plane substrate, the Raman peaks signal intensity of RhB scattered from the SERS substrate are found to be enhanced by several orders when detected with the spectrometer. The EF of the proposed substrate is calculated using equation 1.22. I_{SERS} and I_{REF} are obtained from the recorded data corresponding to Raman peak at 1282 cm^{-1} which is attributed to C-H bending. The enhancement factor is calculated to be 3.27×10^8 corresponding to this specific peak. Other prominent signature peaks at 414 cm^{-1} and 886 cm^{-1} correspond to C-N-C bend and C-H out of plane deformation respectively.

Minimum measurable sample concentration

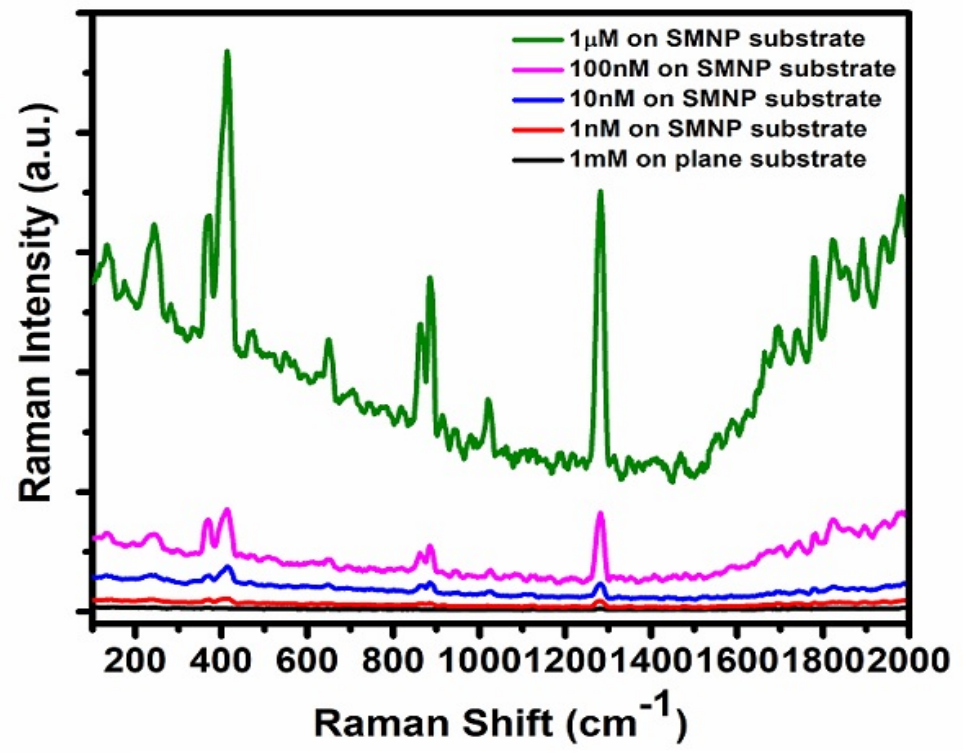

Figure 2.9: SERS spectra of RhB at different concentrations. For all concentrations, the exciting laser of wavelength 785 nm and output power has been kept constant.

To find out the minimum sample concentration that can be detected reliably with the proposed SERS substrate, four different concentrations 1 μM, 100 nM, 10 nM and 1 nM of RhB samples are considered for the study. The samples are treated on the SERS substrate and allowed to dry in room temperature environment for two hours. The scattered Raman signals are then recorded by the Raman spectrometer and corresponding result is shown in figure 2.9. For reference Raman signal intensity scattered from a plane silicon substrate of 1 mM RhB is also included in the same figure. It is clearly seen that with the decrement of sample concentration, the signature Raman peaks intensities of the sample also decreases proportionately. In the present study, the minimum concentration of RhB that can be recorded reliably by the spectrometer is 1nM.

Reproducibility of the substrate

The reproducibility of SERS substrate is an important sensoristic characteristic to be evaluated for any SERS based sensing study. To study this parameter, the designed substrate has been treated with 10 μL of 1 μM RhB solution, and upon drying of the

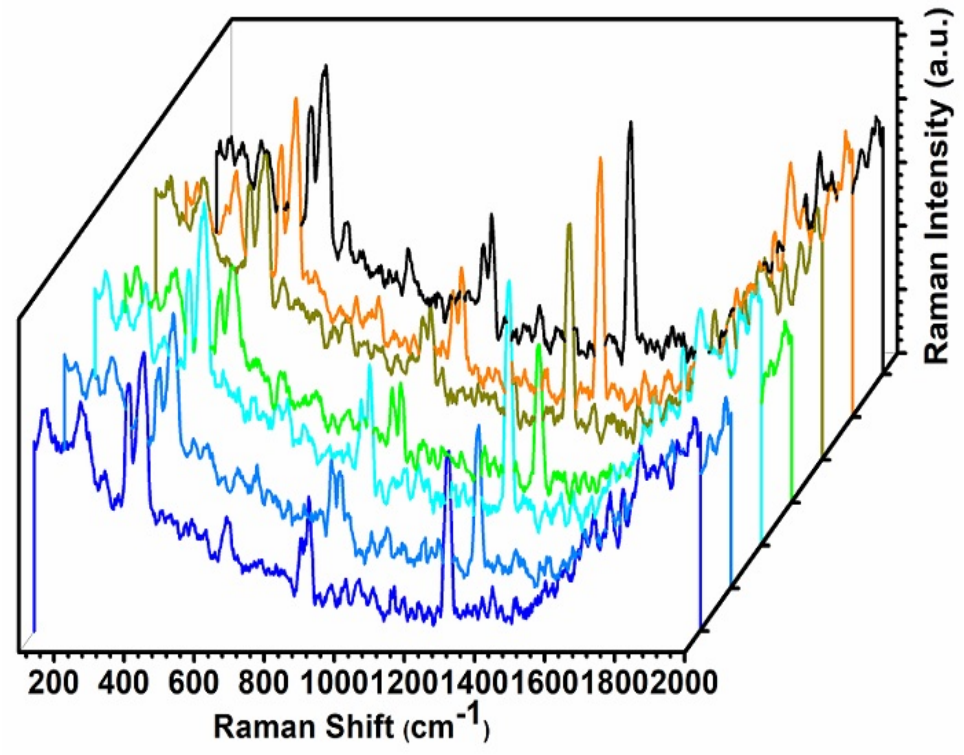

Figure 2.10: Raman spectra of 1 μM RhB solution at seven different locations on the DASAuNP substrate.

sample the back-scattered Raman signal has been recorded from seven randomly selected positions from the sensing region of the substrate. Figure 2.10 shows the characteristic Raman signals recorded by the spectrometer scattered from the considered locations of the substrate. The peak signal intensity corresponding to Raman shift at 1282 cm^{-1} is observed to be fluctuated with relative standard deviation (RSD) value of 13 %. The hot spot density of SERS substrate plays a crucial role in estimating the enhancement of the Raman signal. In the designed substrate, the hot spot density is calculated to be 2.45×10^7 /mm^2. This order is significantly higher than its counterparts already reported elsewhere [25-27]. Although the designed SERS substrate has been fabricated on a silica substrate, the same metal nanostructured pattern can be developed on a low-cost plastic sheet using nanoreplica molding technique. The metal nanopatterned plastic sheet can be used as a disposable SERS substrate.

2.5 Summary

A simulation study for two different metal nanostructures and realization of SERS substrate from one of the simulated structure have been carried out in this chapter. As com-

pared to uniformly structured Au nanopillar, periodically varying height Au nanopillar yields relatively enhanced LSPR field conditions over the patterned region. By controlling pillar height difference, pillar diameter and spacing in the structure, a highly enhanced LSP field condition can be achieved with enhancement factor of 1.32 as compared to the uniformly patterned counterparts. The EF of the fabricated DASAuNP SERS substrate is calculated to be 3.27×10^8. The patterned substrate yields a good degree of reproducibility characteristics with maximum RSD value is observed to be 13%. Using replica molding technique the designed pattern can be produced in mass scale on low-cost plastic sheet and can be used as disposable SERS substrate for sensing of important chemicals and biological samples.

References

[1] Wang, P., Pang, S., Chen, J., McLandsborough, L., Nugen, S. R., Fan, M., and He, L. Label-free mapping of single bacterial cells using surface-enhanced raman spectroscopy. *Analyst,* 141(4):1356-1362, 2016.

[2] Willets, K. A. and Van Duyne, R. P. Localized surface plasmon resonance spectroscopy and sensing. *Annu. Rev. Phys. Chem.,* 58:267-297, 2007.

[3] Haes, A. J., Stuart, D. A., Nie, S., and Van Duyne, R. P. Using solution-phase nanoparticles, surface-con

ned nanoparticle arrays and single nanoparticles as biological sensing platforms. *Journal of Fluorescence,* 14(4):355-367, 2004.

[4] Yonzon, C. R., Stuart, D. A., Zhang, X., McFarland, A. D., Haynes, C. L., and Van Duyne, R. P. Towards advanced chemical and biological nanosensors-an overview. *Talanta,* 67(3):438-448, 2005.

[5] Anker, J. N., Hall, W. P., Lyandres, O., Shah, N. C., Zhao, J., and Van Duyne, R. P. Biosensing with plasmonic nanosensors. In *Nanoscience And Technology: A Collection of Reviews from Nature Journals,* 308-319. World Scientific, 2010.

[6] Brolo, A. G. Plasmonics for future biosensors. *Nature Photonics,* 6(11):709, 2012.

[7] Sepúlveda, B., Angelomé, P. C., Lechuga, L. M., and Liz-Marzán, L. M. Lspr-based nanobiosensors. *nano today,* 4(3):244-251, 2009.

[8] Jans, H. and Huo, Q. Gold nanoparticle-enabled biological and chemical detection and analysis. *Chemical Society Reviews,* 41(7):2849-2866, 2012.

[9] Wu, H.-Y., Choi, C. J., and Cunningham, B. T. Plasmonic nanogap-enhanced raman scattering using a resonant nanodome array. *Small,* 8(18):2878-2885, 2012.

[10] Choi, C. J., Xu, Z., Wu, H.-Y., Liu, G. L., and Cunningham, B. T. Surface-enhanced raman nanodomes. *Nanotechnology,* 21(41):415301, 2010.

[11] Guillot, N., Shen, H., Frémaux, B., Péron, O., Rinnert, E., Toury, T., and Lamy de la Chapelle, M. Surface enhanced raman scattering optimization of gold nanocylinder arrays: Influence of the localized surface plasmon resonance and excitation wavelength. *Applied Physics Letters,* 97(2):023113, 2010.

[12] Choi, C. J. and Semancik, S. Multi-resonant plasmonic nanodome arrays for label-free biosensing applications. *Nanoscale,* 5(17):8138-8145, 2013.

[13] Kuo, C.-W., Shiu, J.-Y., and Chen, P. Size-and shape-controlled fabrication of large-area periodic nanopillar arrays. *Chemistry of materials,* 15(15):2917-2920, 2003.

[14] Kuo, C.-W., Shiu, J.-Y., Chen, P., and Somorjai, G. A. Fabrication of size-tunable largearea periodic silicon nanopillar arrays with sub-10-nm resolution. *The Journal of Physical Chemistry B,* 107(37):9950-9953, 2003.

[15] Caldwell, J. D., Glembocki, O., Bezares, F. J., Bassim, N. D., Rendell, R. W., Feygelson, M., Ukaegbu, M., Kasica, R., Shirey, L., and Hosten, C. Plasmonic nanopillar arrays for large-area, high-enhancement surface-enhanced raman scattering sensors. *ACS nano,* 5(5):4046-4055, 2011.

[16] Li, L., Fang Lim, S., Puretzky, A. A., Riehn, R., and Hallen, H. Near-field enhanced ultraviolet resonance raman spectroscopy using aluminum bow-tie nano-antenna. *Applied physics letters,* 101(11):113116, 2012.

[17] Eskelinen, A.-P., Moerland, R. J., Kostiainen, M. A., and Törmä, P. Self-assembled silver nanoparticles in a bow-tie antenna configuration. *Small,* 10(6):1057-1062, 2014.

[18] Wang, X., Li, Y., Wang, H., Fu, Q., Peng, J., Wang, Y., Du, J., Zhou, Y., and Zhan, L. Gold nanorod-based localized surface plasmon resonance biosensor for sensitive detection of hepatitis b virus in buffer, blood serum and plasma. *Biosensors and Bioelectronics,* 26(2):404-410, 2010.

[19] Multiphysics, C. Comsol multiphysics user guide (version 4.3 a). *COMSOL, AB,* 39-40, 2012.

[20] Chung, T., Lee, S.-Y., Song, E. Y., Chun, H., and Lee, B. Plasmonic nanostructures for nano-scale bio-sensing. *Sensors,* 11(11):10907-10929, 2011.

[21] Liu, J., Zhang, S., Ma, Y., Shao, J., Lu, B., and Chen, Y. Gold nanopillar arrays as biosensors fabricated by electron beam lithography combined with electroplating. *Applied optics,* 54(9):2537-2542, 2015.

[22] Liu, J., Ma, Y., Shao, J., Zhang, S., and Chen, Y. Ultra-tall sub-wavelength gold nano pillars for high sensitive lspr sensors. *Microelectronic Engineering,* 196:7-12, 2018.

[23] Johnson, P. B. and Christy, R.-W. Optical constants of the noble metals. *Physical review B,* 6(12):4370, 1972.

[24] Liao, P. and Wokaun, A. Lightning rod effect in surface enhanced raman scattering. *The Journal of Chemical Physics,* 76(1):751-752, 1982.

[25] Wu, H.-Y., Choi, C. J., and Cunningham, B. T. Plasmonic nanogap-enhanced raman scattering using a resonant nanodome array. *Small,* 8(18):2878-2885, 2012.

[26] Jensen, T. R., Malinsky, M. D., Haynes, C. L., and Van Duyne, R. P. Nanosphere lithography: tunable localized surface plasmon resonance spectra of silver nanoparticles. *The Journal of Physical Chemistry B,* 104(45):10549-10556, 2000.

[27] Zhang, J., Irannejad, M., and Cui, B. Bowtie nanoantenna with single-digit nanometer gap for surface-enhanced Raman scattering (SERS). *Plasmonics,* 10(4):831-837, 2015.